Mead Silvester, J.; Lenn, Yueng-Djern; Polton, Jeff A.; Rippeth, Tom P.; Morales Maqueda, M.. 2014 Observations of a diapycnal shortcut to adiabatic upwelling of Antarctic Circumpolar Deep Water. *Geophysical Research Letters*, 41 (22). 7950-7956. 10.1002/2014GL061538

Mead Silvester, J.; Lenn, Yueng-Djern; Polton, Jeff A.; Rippeth, Tom P.; Morales Maqueda, M.. 2014 Observations of a diapycnal shortcut to adiabatic upwelling of Antarctic Circumpolar Deep Water. *Geophysical Research Letters*, 41 (22). 7950-7956. 10.1002/2014GL061538

AGU PUBLICATIONS

Geophysical Research Letters

RESEARCH LETTER

10.1002/2014GL061538

Key Points:
- Intermittent dissipation events of O(10^{-6}) W kg^{-1} captured by VMP measurements
- Events occur between adjacent upwelling and downwelling Southern Ocean MOC limbs
- Upwelling waters may shortcut adiabatic upwelling pathways via diapycnal mixing

Correspondence to:
J. Mead Silvester,
j.mead.silvester@bangor.ac.uk

Citation:
Mead Silvester, J., Y.-D. Lenn, J. A. Polton, T. P. Rippeth, and M. Morales Maqueda (2014), Observations of a diapycnal shortcut to adiabatic upwelling of Antarctic Circumpolar Deep Water, *Geophys. Res. Lett.*, *41*, 7950–7956, doi:10.1002/2014GL061538.

Received 28 AUG 2014
Accepted 20 OCT 2014
Accepted article online 22 OCT 2014
Published online 25 NOV 2014

Observations of a diapycnal shortcut to adiabatic upwelling of Antarctic Circumpolar Deep Water

J. Mead Silvester[1,2], Yueng-Djern Lenn[2], Jeff A. Polton[1], Tom P. Rippeth[2], and M. Morales Maqueda[1]

[1]National Oceanography Centre, Liverpool, UK, [2]School of Ocean Sciences, Bangor University, Menai Bridge, UK

Abstract In the Southern Ocean, small-scale turbulence causes diapycnal mixing which influences important water mass transformations, in turn impacting large-scale ocean transports such as the Meridional Overturning Circulation (MOC), a key controller of Earth's climate. We present direct observations of mixing over the Antarctic continental slope between water masses that are part of the Southern Ocean MOC. A 12 h time series of microstructure turbulence measurements, hydrography, and velocity observations off Elephant Island, north of the Antarctic Peninsula, reveals two concurrent bursts of elevated dissipation of $O(10^{-6})$ W kg^{-1}, resulting in heat fluxes ~10 times higher than basin-integrated Drake Passage estimates. This occurs across the boundary between adjacent adiabatic upwelling and downwelling overturning cells. Ray tracing to nearby topography shows mixing between 300 and 400 m is consistent with the breaking of locally generated internal tidal waves. Since similar conditions extend to much of the Antarctic continental slope where these water masses outcrop, diapycnal mixing may contribute significantly to upwelling.

1. Introduction

The global overturning circulation, a critical component of the Earth's climate system, transports heat gained in the tropics to high latitudes, where it is lost to the atmosphere [*Wunsch and Ferrari*, 2004; *Marshall and Speer*, 2012]. This circulation is sustained by ~2 TW of mechanical energy input, of which approximately half comes from atmospheric winds and half from tides [*Munk*, 1966]. Tide and wind energy force internal waves which dissipate energy to small-scale turbulence in vertical mixing events. The vertical exchange of heat and mass in the abyssal ocean balances deep water formation at high latitudes, maintaining abyssal stratification [*Wunsch and Ferrari*, 2004]. However, observed background dissipation of $O(10^{-10})$ W kg^{-1} is insufficient to fully balance deep water formation, suggesting that intense vertical mixing is concentrated in a few locations [*Naveira Garabato et al.*, 2004]. The Southern Ocean, the key place where waters subducted or convected elsewhere rise to the surface to close the MOC, has recently come into focus as one such region of concentrated vertical mixing. Approximately 80% of the planet's wind energy is bound in storm tracks over the Southern Ocean [*Zhai et al.*, 2012] and this, coupled with topographic roughness and the action of tides, makes the Southern Ocean a potential hot spot for diapycnal mixing [*Egbert*, 2004; *Watson et al.*, 2013; *Wu et al.*, 2011].

This study focuses on Drake Passage, a topographically complex chokepoint for ocean currents where elevated levels of tidally forced diapycnal mixing can be expected [*Heywood et al.*, 2007; *Padman et al.*, 2006]. Our measurements are taken to the north of Elephant Island, at the northern tip of the Antarctic Peninsula (Figure 1a). M_2 tidal amplitudes [*Padman et al.*, 2002] and topographic roughness [*Wu et al.*, 2011] in the vicinity of Elephant Island are typical of the Antarctic continental shelf break equatorward of the M_2 critical latitude (~74.5°S), accounting for ~60% of the continental slope. At these latitudes, important water transformations occur as deep waters are drawn to the surface along tilting isopycnals where they are either transported northward by Ekman transports to form Antarctic Intermediate Water (AAIW) or South Antarctic Mode Water (SAMW), or lose buoyancy through air-sea fluxes near the cold continent and sink to form Antarctic Bottom Water (AABW) [*Sloyan and Rintoul*, 2001] (Figure 1b). Although these transformations do not occur over all longitudes in the Southern Ocean, Drake Passage is close to the site of Atlantic AAIW/SAMW formation [*Piola and Gordon*, 1989], and immediately to the north of Elephant Island, dense waters formed along the eastern side of the Antarctic Peninsula convect downslope [*Meredith et al.*, 2003]. While the return of deep waters to the surface along outcropping, inclined isopycnals is thought to dominate Southern Ocean upwelling, it has been suggested that such adiabatic processes are unable to account

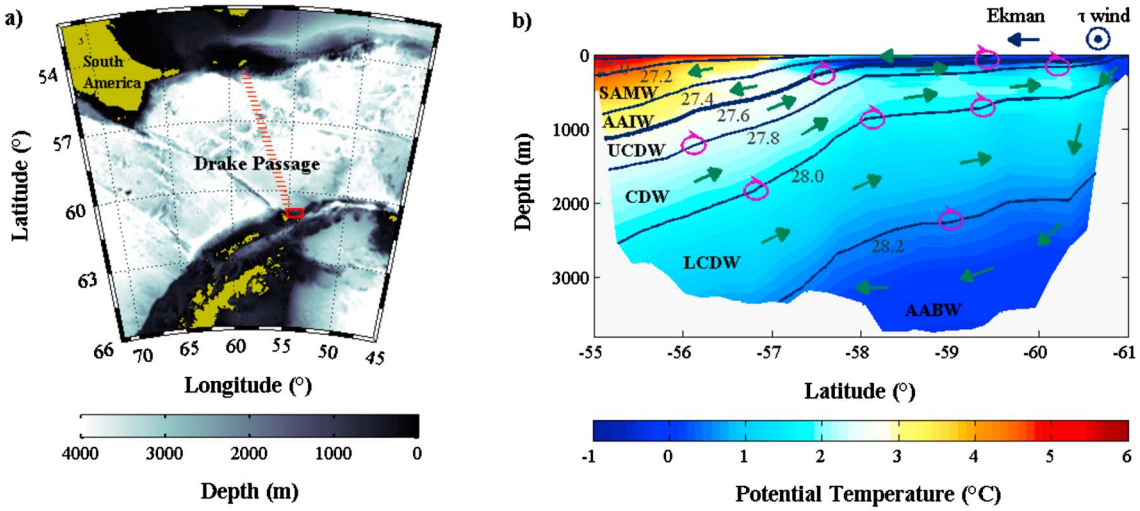

Figure 1. (a) The location of the study site near Elephant Island is delimited by the red box. The red track marks the conductivity-temperature-depth (CTD) transect across Drake Passage, (b) the hydrography from which is used to construct schematic to illustrate meridional water mass transports across Drake Passage. Potential density (ρ − 1000 kg m^{-3}) is contoured, with the thicker line marking (isopycnal σ = 27.6 kg m^{-3}) the boundary between upwelling and downwelling cells of the Southern Ocean MOC. Green arrows show the mean overturning circulation: wind-driven northward Ekman transport, northward spread of waters cooled at the surface and sinking to form Antarctic Bottom Water (AABW) are all replenished by Circumpolar Deep Waters (CDW), Upper CDW (UCDW), and Lower CDW (LCDW) via adiabatic upwelling along isopycnals [e.g., *Marshall and Speer*, 2012; *Sloyan and Rintoul*, 2001]. Subantarctic Mode Water (SAMW) and Antarctic Intermediate Water (AAIW) are also formed within the Southern Ocean from subducting deep winter mixed layers. Pink recirculating arrows illustrate diapycnal mixing, a potential means for upwelling waters to short-circuit adiabatic pathways.

entirely for upward volume transports in the Southern Ocean, implicating diapycnal mixing as a contributor [*Naveira Garabato et al.*, 2007]. *Watson et al.* [2013] estimate from a tracer dispersion experiment that diapycnal mixing drives 20–30% of total Southern Ocean upwelling. We present the first time series of direct dissipation measurements to resolve strong intermittent diapycnal mixing episodes within the southernmost extent of Upper Circumpolar Deep Waters (UCDW), north of Elephant Island.

2. Measurements and Methods

From 18 to 29 November 2009, RRS *James Clark Ross* carried out a microstructure turbulence time series (JR198) and the annually repeated SR1B hydrographic survey from Burdwood Bank (south of the Falkland Islands) to Elephant Island across Drake Passage. Thirty-one full-depth conductivity-temperature-depth (CTD) stations were completed during the survey, culminating in a 12 h station during which a free falling Rockland Scientific Instruments vertical microstructure profiler VMP-1000 (VMP hereafter), measuring turbulent kinetic energy (TKE) dissipation rates, repeatedly profiled off the northern coast of Elephant Island on 25 November (Figures 1a and 2a). The VMP was equipped with microstructure shear probes, temperature and conductivity sensors and profiled simultaneously with a SeaBird Electronics CTD for independent, calibrated temperature and conductivity measurements. Fourteen such casts were accomplished, each approximately 800 m deep and taking 50 min from deployment to recovery. A shipboard 75 kHz RDI Ocean Surveyor acoustic Doppler current profiler (ADCP) measured velocities in 16 m bins with the first centered at a depth of 46.24 m, with bottom tracking off during the microstructure measurements, and was calibrated using water track data during postprocessing into along- (u) and across-slope (v) components. The barotropic tide is estimated from TPXO7.2 [*Egbert et al.*, 1994] with the timing of high tide agreeing precisely with local bottom pressure recordings from Antarctic Circumpolar Current Levels by Altimetry and Island Measurements (ACCLAIM) data.

From ADCP velocities, square of shear was computed as the change in u and v velocity with depth, squared. Turbulent diffusivity is estimated using Osborn's relation [*Osborn*, 1980] as $K_\rho = \Gamma \frac{\varepsilon}{N^2}$, where ε is the dissipation rate from direct VMP measurements, buoyancy frequency N^2 is calculated from simultaneous CTD casts, and Γ, the efficiency, is taken to be 0.2. The Ozmidov length scale is computed as $\left(\frac{\varepsilon}{N^3}\right)^{1/2}$, where N is the Brunt-Väisälä frequency. The M_2 ray slope $\left(\alpha = \sqrt{\frac{\omega^2 - f^2}{\langle N \rangle^2 - \omega^2}}\right)$ is calculated from the internal wave

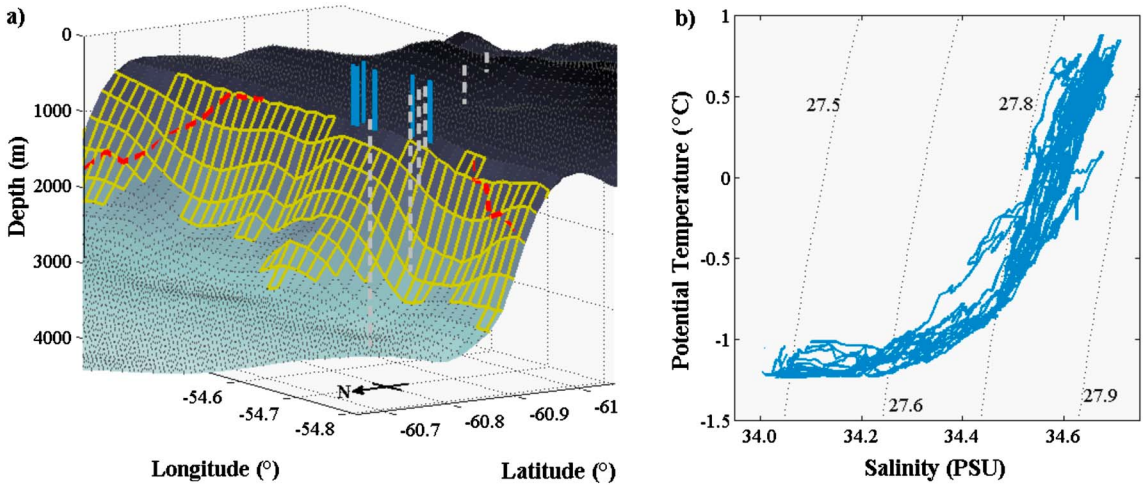

Figure 2. (a) Nearby transect CTD stations (white dashed lines) and VMP-CTD casts (solid blue profiles) are superimposed upon topography [*Amante and Eakins*, 2009] using the same color scheme as (Figure 1a) as a reference to the bathymetry of the wider area. Casts drifted from west to east (right to left) along the shelf. Coordinate cells highlighted in yellow demarcate critical slopes according to the Baines parameter ($0.5 < \gamma > 2.0$) and thick, dashed red lines show the intersection of the M_2 ray path with critically sloped topography. (b) Temperature-salinity diagram.

dispersion relation where $\omega = 2\pi/12.42\ \mathrm{h}^{-1}$ is the frequency of the M_2 tide; $f = -1.2737 \times 10^{-4}\ \mathrm{s}^{-1}$ is the Coriolis parameter at this latitude; angle brackets denote time-averaged values; N^2 is derived from CTD casts corresponding to VMP casts for the upper 800 m of the water column and, below 800 m, from the final five ship's CTD transect stations (Figure 2a). The Baines parameter is computed according to $\gamma = \frac{\mathrm{d}H/\mathrm{d}y}{\alpha}$ [*Baines*, 1982], where $\mathrm{d}H/\mathrm{d}y$ represents the topographic slope in the ray propagation direction. Finally, the conversion of lee-wave energy flux to diapycnal heat flux is calculated after *Huang* [1999] as $F = \frac{cbE/H}{g\alpha_w}$, where $c = 4181\ \mathrm{J\ kg}^{-1}$ is the specific heat capacity of water; b is the fraction of mechanical energy used for mixing and is of the order 0.1; E is the mechanical energy flux; H is the depth of the water column; $g = 9.8\ \mathrm{m\ s}^{-2}$ is the acceleration due to gravity; and $\alpha_w = 0.167 \times 10^{-3}\ \mathrm{K}^{-1}$ is the thermal expansion coefficient of water.

3. Results

Direct measurements of energy dissipation rates fall within the southernmost reaches of shoaling UCDW where it is drawn to the surface over the Antarctic continental slope. Here northeastward flowing currents dominate, following the shelf edge and the curve of the Antarctic Peninsula. At the VMP station, the shelf edge is approximately aligned in an east-west orientation (Figures 1a and 2a), with a dominant eastward flow. The hydrographic CTD section is oriented in an across-slope sense with the VMP and simultaneous CTD casts aligned along-slope due to ship drift and is confined within a 3 km^2 area (Figure 2a). Analyses of temperature and salinity characteristics show a water mass of consistent properties at the margins of the UCDW class (Figure 2b), with negligible variation along the slope relative to that across the slope. In zonal averages, isopcynal $\sigma = 27.6\ \mathrm{kg\ m}^{-3}$ delineates the upper and lower Southern Ocean MOC cells [*Lumpkin and Speer*, 2007]. In a 10 year averaged SR1b hydrographic section (Figure 1b), UCDW ranges from $\sigma = 27.6\ \mathrm{kg\ m}^{-3}$ to $\sigma = 27.8\ \mathrm{kg\ m}^{-3}$ with LCDW and the lower overturning cell found at higher densities.

3.1. Turbulent Kinetic Energy Dissipation, Mixing, and Stratification

The VMP observations were collected over a 12 h period with the intention of resolving the semidiurnal tide (Figure 3a). During this period, the surface tide cycled approximately from low through high to low water (Figure 3b) with tidal current amplitudes of $u < 7\ \mathrm{cm\ s}^{-1}$ and $v < 2\ \mathrm{cm\ s}^{-1}$.

Relative to background dissipation levels of $O(10^{-9})\ \mathrm{W\ kg}^{-1}$, two separate bursts of elevated turbulent dissipation $O(10^{-6})\ \mathrm{W\ kg}^{-1}$ were recorded between 16:30 and 19:00 UTC (casts 7–9), at depths of 120–200 m and 300–400 m. Relative to isopycnals, the upper patch of intense dissipation maintained a thickness of 25–30 m and shoaled progressively; the lower burst was confined between constant depths. Both persisted for approximately 2 h, sampled by three consecutive VMP profiles. Isopycnals immediately below the lower dissipation event ($\sigma = 27.8\ \mathrm{kg\ m}^{-3}$) were displaced by 70–80 m, with the largest amplitude

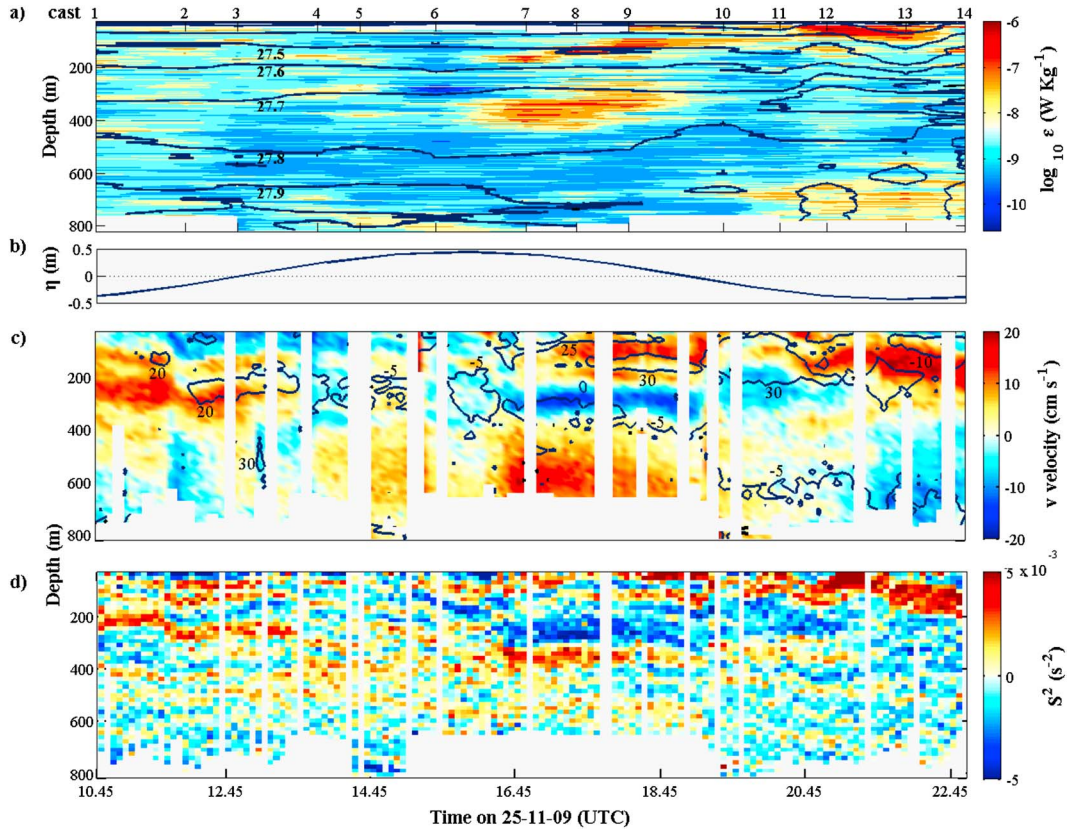

Figure 3. (a) Time series of the TKE dissipation rate, ε, from VMP casts with black contoured lines demarcating potential density ($\rho - 1000$ kg m^{-3}) measured by simultaneous CTD casts. (b) Surface elevation due to semidiurnal M_2 tidal constituent from TPXO7.2. (c) ADCP measurements of absolute v velocity in color-filled contours with u velocity contours overlain in black, both with the depth-mean velocity subtracted. (d) Bin-by-bin squared shear (S^2) computed from ADCP velocity data.

displacement coinciding with the maximum surface elevation of the semidiurnal barotropic tide. Peak eddy diffusivities, K_ρ, of $\sim 6 \times 10^{-3}$ m^2 s^{-1} and $\sim 1 \times 10^{-3}$ m^2 s^{-1} compared with background diffusivities of $<0.1 \times 10^{-3}$ m^2 s^{-1} coincide with upper and lower bursts of dissipation, respectively (Figures 4a and 4b). Mixing events dominate the vertical heat flux at these depths averaging 25 ± 18 W m^{-2} during the upper burst and 58 ± 36 W m^{-2} during the lower event, significantly higher than average background levels of 3 ± 1 W m^{-2} and 4 ± 2 W m^{-2}, respectively.

3.2. Current Velocities

The u and v velocity components, aligned in the along- and across-slope directions, respectively, reveal a strong reversal in across-slope current direction at 250–300 m depth, coincident with the timing of middepth dissipation events (Figure 3c). This current reversal coincides temporally with isopycnic heave (Figure 3a). The signature of the middepth v velocity reversal is clearly visible in the square of shear (Figure 3d).

4. Discussion

This investigation focuses on the two distinctive bursts of dissipation $O(10^{-6})$ W kg^{-1}, which are $O(10^3)$ larger than background dissipation levels observed at middepths. Other instances of elevated dissipation were also captured, notably in the surface layer (casts 12–14) and the bottom boundary layer (casts 4–6; 11–14) with analyses (not shown) revealing that near-surface mixing is consistent with shear spiking from inertial energy input [*Brannigan et al.*, 2013] and that mixing lower in the water column may be attributed to bottom boundary layer processes, but their treatment is beyond the scope of this paper. Instead, the discussion is centered on elevated dissipation at middepths where upwelling occurs. Specifically, we speculate as

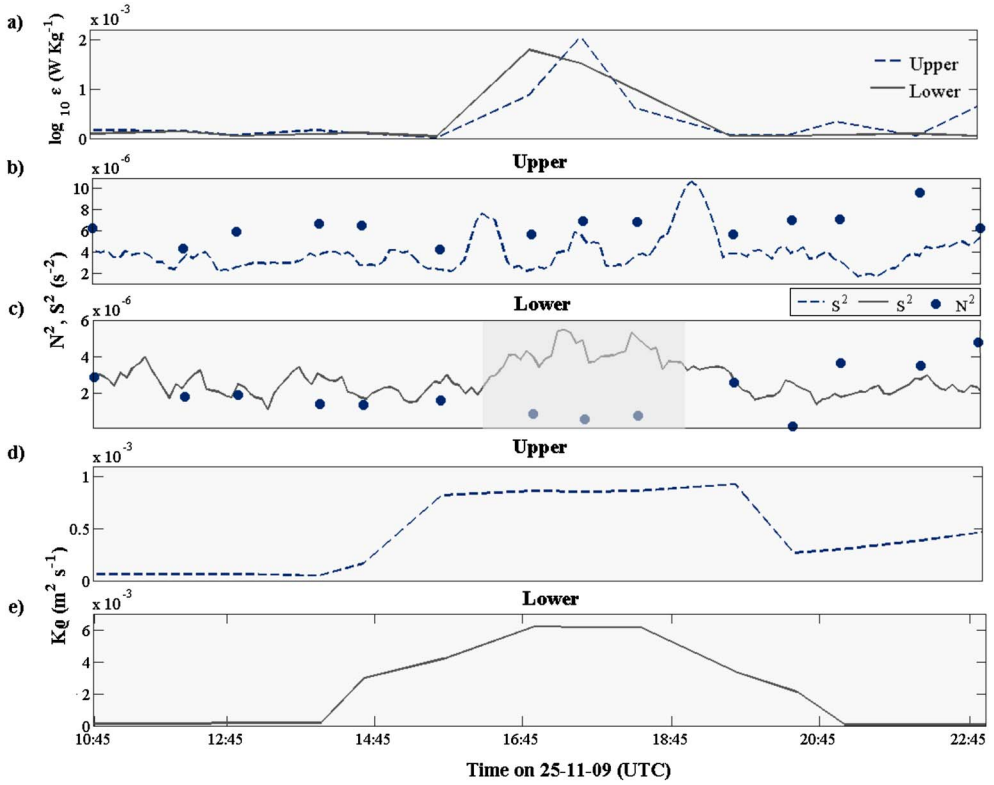

Figure 4. (a) Total dissipation between 120–200 m (upper) and 300–400 m (lower). (b and c) Buoyancy frequency, N^2 (dots), and squared shear, S^2 (lines), for upper (dashed lines) and lower (solid lines) bursts of dissipation, with the period where the Richardson number $N^2/S^2 < 0.25$ shaded in Figure 4c. (d and e) Estimated mean turbulent diffusivity between 120–200 m and 300–400 m, coincident with upper and lower bursts of dissipation, respectively.

to the origin of the energy available for driving turbulent dissipation and discuss the implications of these dissipation bursts on diapycnal mixing.

Of the upper and lower bursts of dissipation, the latter is associated with a greater diffusivity, K_ρ, of $\sim 6 \times 10^{-3}$ m^2 s^{-1} above background levels compared to $\sim 1 \times 10^{-3}$ m^2 s^{-1} in the upper case, where the rise in dissipation is accompanied by an increase in stratification (Figure 4). This is reinforced by comparing the mean square of shear, S^2, and N^2 across the layers containing high dissipation. This comparison reveals that the Richardson number falls to <0.25 during the lower dissipation burst only (Figure 3c), so that only in this instance do the observations indicate that shear is sufficient to overcome stratification in turbulent mixing events. Shear instability may be driving the upper dissipation burst as well, but the Richardson number calculation is compromised by the low vertical resolution (16 m bins) of the 75 kHz ADCP which smooths higher in situ shear as the Ozmidov length scale during the upper burst is much smaller than bin depth (~3 m) but sufficiently large during the lower burst (~15 m).

Three sources known to force the breaking of waves within the internal wave field are investigated: wind, tide, and mesoscale eddies. Comparing the magnitude and alignment of bulk shear vectors across the strata containing high dissipation and the wind stress vector shows that directly wind-driven shear spiking is unlikely to have provided the energy for middepth dissipation (not shown). Temperature and salinity anomalies exhibit no significant correlation with velocity profiles within the velocity reversal periods suggesting that eddies are not responsible for the elevated levels of mixing. Moreover, mesoscale flows vary on timescales of days and longer, further reducing the likelihood of eddies as the cause of this feature. Several features indicative of a tidal signature cannot be conclusively resolved by observations that span only a single semidiurnal period. Nevertheless, the isopycnic displacement occurs at close to the frequency of the M_2 tide (Figures 3a and 3b), and there is a strong sinusoidal signal in the prominent v reversal close to the frequency of the semidiurnal tide (Figures 3b and 3c). Tidal models [*Egbert*, 2004; *Simmons et al.*, 2004;

Padman et al., 2006] implicate the region as a globally significant dissipative site, while *Heywood et al.* [2007] show that internal tides are likely to be generated in Drake Passage from observations of tide-topography interactions but emphasize their elusive detection there.

Internal tides are typically generated from the interaction of the tidal current with sufficiently sloped topography, propagating away from the generation site in a tidal ray refracted through the stratified ocean. Much of the sloped shelf edge north of Elephant Island is critical ($0.5 < \gamma < 2.0$) according to the Baines parameter categorization of *Robertson* [2001], where $\gamma < 0.5$ is subcritical, $\gamma > 2.0$ is supercritical, and a critical slope is the most likely to generate internal tides. Calculating the M_2 ray slope and tracing a radial path from the lower dissipative event to intersect with topography allows us to speculate as to whether locally generated internal tides could have been the driver of observed diffusivity. Assuming no reflection from the seabed, the sites where the M_2 raypath intersects critically sloped topography are shown in Figure 2a. It is suggested that observed middepth turbulent diffusivity is consistent with the breaking of locally generated internal waves forced by the tide.

Our background diffusivities near Elephant Island are directly comparable to basin-integrated estimates (based on tracer dispersion) of diapycnal diffusivity within Drake Passage UCDW by *Watson et al.* [2013] at $3.6 \pm 0.6 \times 10^{-4}$ m^2 s^{-1}, itself an order of magnitude higher than open ocean background diffusivities. Our time-averaged diffusivities, including elevated dissipation events, are approximately 5 times larger than those associated with lee-wave generation in Drake Passage UCDW [*Watson et al.*, 2013], highlighting the importance of continental slope regions for diapycnal mixing.

Large heat fluxes of 25 ± 18 W m^{-2} and 58 ± 36 W m^{-2} resulting from upper and lower dissipation bursts, respectively, are at least an order of magnitude greater than time series background fluxes of 3 ± 1 W m^{-2} and 4 ± 2 W m^{-2}. Consequently, dissipation bursts dominate the time series-averaged fluxes of 8 ± 4 W m^{-2} (upper) and 16 ± 8 W m^{-2} (lower). These heat fluxes, compared with fluxes of ~0.4 W m^{-2} across isopycnal $\sigma = 27.4$ kg m^{-3} in the Atlantic sector of the Southern Ocean (computed using transports of 4×10^6 m^3 s^{-1} and $\Delta T \approx 2.5$°C from *Sloyan and Rintoul* [2001]), are very large. Although this comparison is made across a different isopycnal than that which our fluxes straddle ($\sigma = 27.6$ kg m^{-3}), it is globally representative of the boundary between water masses we observe to have modified properties locally and is the most relevant of the scarce historical estimates for mixing in the Southern Ocean. From the basin-integrated lee-wave energy flux of 0.02 W m^{-2} given for Drake Passage UCDW in *Watson et al.* [2013], the equivalent heat flux is calculated after *Huang* [1999] to be ~5 W m^{-2}, assuming a depth of 1000 m. This is comparable with our background fluxes, while our peak fluxes are ~10 times larger.

The presence of high dissipation rates suggests that diapycnal mixing plays a role in the transformation of upwelling UCDW at Elephant Island. While the prevailing view that the primary mechanism for upwelling in the Southern Ocean, the wind-driven adiabatic transport of mass along inclined, outcropping, and narrowing isopycnals requires no energy to be dissipated [*Marshall and Speer*, 2012], adiabatic pathways are unable to account entirely for upward volume transports here. It has been proposed that vertical mixing across isopycnals and indeed between adjacent upwelling and downwelling water masses is a means of short-circuiting adiabatic upwelling [*Naveira Garabato et al.*, 2007]. Our observations provide evidence for the presence of strong intermittent diapycnal mixing, where adiabatic upwelling occurs, across isopycnals that generally divide the upper and lower Southern Ocean MOC cells (approximately $\sigma = 27.6$ kg m^{-3}) in a circumpolar sense. Mixing within the water masses at the interface of the two Southern Ocean overturning cells may allow water mass transformation to occur at depth instead of at the surface following adiabatic upwelling. These isopycnals typically outcrop between ~60°S and ~70°S, approaching the Antarctic continental slope along the Antarctic Peninsula and between ~45°E and ~145°E, south of Australia [*Marshall and Speer*, 2012]. Given that similar topographic roughness and M_2 tidal amplitudes extend to ~60% of the Antarctic continental slope and coincide with where the outcropping of UCDW and LCDW approaches the slope, intermittent, tidally driven mixing across the UCDW-LCDW interface may also occur elsewhere.

Although limited to narrow shelf break regions and intermittent, such elevated diapycnal mixing may drive the missing middepth water mass transformation of *Watson et al.* [2013], influencing our understanding of Southern Ocean overturning strength. The broad implications of diapycnal mixing at this location for Southern Ocean water mass transformations and upwelling rates drawn from this short time series deserve further investigation, and it is significant that we have identified a place where this can be studied.

5. Conclusions

A 12 h time series of TKE dissipation rates in which we observe elevated intermittent mixing across the boundary between adjacent adiabatically upwelling and downwelling branches of the Southern Ocean MOC is investigated. Two concurrent bursts of elevated dissipation of $O(10^{-6})$ W kg^{-1} between 120–200 m and 300–400 m are associated with high diffusivity and significant vertical heat fluxes that dominate time series average fluxes of 8 ± 4 W m^{-2} and 16 ± 8 W m^{-2} and are significantly higher than regional estimates. The lower event appears consistent with the breaking of locally generated internal tidal waves through shear instability. Our observations provide evidence that intermittent diapycnal mixing has led to large heat fluxes in upwelling regions. While the contribution of diapycnal mixing to upwelling per se at this location has not been quantified, the mixing of tracers has implications for water mass transformations. Yet if intermittent diapycnal mixing at such key locations has the potential to influence upwelling rates, and moreover, if it occurs elsewhere along the Antarctic continental slope, this may have far-reaching consequences for the strength of the MOC. This short time series demonstrates the importance of continental slope regions for diapycnal mixing and identifies a place where the contributions of adiabatic and diapycnal mixing processes to upwelling should be studied. Finally, the large range in heat fluxes over the time series highlights the need for further studies resolving variation on subinertial and subtidal timescales to elicit underlying processes.

Acknowledgments

We thank the officers and crew of the RRS *James Clark Ross* and the British Antarctic Survey IT and ETS personnel for their support during the science cruises JR195 and JR198. This work was carried out under the auspices of NERC's National Capability project, ACCLAIM. Additionally, J.M.S. was supported by NERC studentship (NE/K500938/1); Y.D.L. by NERC Fellowship (NE/H016007/1); J.P. by NOC Modelling National Capability, FASTNEt (NE/I030259/1) and Irish Sea Observatory National Capability; M.A.M.M. by OSCAR (NE/I022868/1); and T.P.R. by TEA-COSI (NE/1029226/1) and OSMOSIS (NE/1019794/1). Data can be requested from the British Oceanographic Data Centre, BODC. Finally, we thank two anonymous reviewers for their constructive comments that led to a substantially improved manuscript.

Lisa Beal thanks two anonymous reviewers for their assistance in evaluating this paper.

References

Amante, C., and B. W. Eakins (2009), ETOPO1 1 arc-minute global relief model: Procedures, data sources and analysis, *NOAA Technical Memorandum NESDIS NGDC*, US Department of Commerce, National Oceanic and Atmospheric Administration, National Environmental Satellite, Data, and Information Service, National Geophysical Data Center, Marine Geology and Geophysics Division.

Baines, P. (1982), On internal tide generation models, *Deep Sea Res., Part A*, *29*(3), 307–338, doi:10.1016/0198-0149(82)90098-X.

Brannigan, L., Y.-D. Lenn, T. P. Rippeth, E. McDonagh, T. K. Chereskin, and J. Sprintall (2013), Shear at the base of the oceanic mixed layer generated by wind shear alignment, *J. Phys. Oceanogr.*, *43*(8), 1798–1810, doi:10.1175/JPO-D-12-0104.1.

Egbert, G. D. (2004), Numerical modeling of the global semidiurnal tide in the present day and in the last glacial maximum, *J. Geophys. Res.*, *109*, 1–15, doi:10.1029/2003JC001973.

Egbert, G. D., A. F. Bennett, and M. G. G. Foreman (1994), TOPEX/POSEIDON tides estimated using a global inverse model, *J. Geophys. Res.*, *99*(C12), 24,821–24,852, doi:10.1029/94JC01894.

Heywood, K. J., J. L. Collins, C. W. Hughes, and I. Vassie (2007), On the detectability of internal tides in Drake Passage, *Deep Sea Res., Part I*, *54*(11), 1972–1984, doi:10.1016/j.dsr.2007.08.002.

Huang, R. X. (1999), Mixing and energetics of the oceanic thermohaline circulation*, *J. Phys. Oceanogr.*, *29*(4), 727–746, doi:10.1175/1520-0485(1999)029<0727:MAEOTO>2.0.CO;2.

Lumpkin, R., and K. Speer (2007), Global ocean meridional overturning, *J. Phys. Oceanogr.*, *37*(10), 2550–2562, doi:10.1175/JPO3130.1.

Marshall, J., and K. Speer (2012), Closure of the meridional overturning circulation through Southern Ocean upwelling, *Nat. Geosci.*, *5*(3), 171–180, doi:10.1038/ngeo1391.

Meredith, M. P., C. W. Hughes, and P. R. Foden (2003), Downslope convection north of Elephant Island, Antarctica: Influence on deep waters and dependence on ENSO, *Geophys. Res. Lett.*, *30*(9), 1462, doi:10.1029/2003GL017074.

Munk, W. H. (1966), Abyssal recipes, *Deep Sea Res.*, *13*(4), 707–730.

Naveira Garabato, A. C., K. L. Polzin, B. A. King, K. J. Heywood, and M. Visbeck (2004), Widespread intense turbulent mixing in the Southern Ocean, *Science*, *303*(5655), 210–213, doi:10.1126/science.1090929.

Naveira Garabato, A. C., D. P. Stevens, A. J. Watson, and W. Roether (2007), Short-circuiting of the overturning circulation in the Antarctic Circumpolar Current, *Nature*, *447*(7141), 194–197.

Osborn, T. R. (1980), Dissipation measurements of oceanic turbulence, in *Marine Turbulence Proceedings of the 11th International Liège Colloquium on Ocean Hydrodynamics*, vol. 28, pp. 143–155, Elsevier, Amsterdam.

Padman, L., H. A. Fricker, R. Coleman, S. Howard, and L. Erofeeva (2002), A new tide model for the Antarctic ice shelves and seas, in *Annals of Glaciology,* vol. 34, pp. 247–254, Int. Glaciol. Soc., Cambridge, U. K., and New York, doi:10.3189/172756402781817752.

Padman, L., S. Howard, and R. Muench (2006), Internal tide generation along the South Scotia Ridge, *Deep Sea Res., Part II*, *53*, 157–171, doi:10.1016/j.dsr2.2005.07.011.

Piola, A. R., and A. L. Gordon (1989), Intermediate waters in the southwest South Atlantic, *Deep Sea Res., Part A*, *36*(1), 1–16, doi:10.1016/0198-0149(89)90015-0.

Robertson, R. (2001), Internal tides and baroclinicity in the southern Weddell Sea: 1. Model description, *J. Geophys. Res.*, *106*, 27,001–27,016.

Simmons, H. L., R. W. Hallberg, and B. K. Arbic (2004), Internal wave generation in a global baroclinic tide model, *Deep Sea Res., Part II*, *51*(25-26), 3043–3068.

Sloyan, B. M., and S. R. Rintoul (2001), The Southern Ocean limb of the global deep overturning circulation, *J. Phys. Oceanogr.*, *31*(1), 143–173, doi:10.1175/1520-0485(2001)031.0143:TSOLOT.2.0.CO;2.

Watson, A. J., J. R. Ledwell, M.-J. Messias, B. A. King, N. Mackay, M. P. Meredith, B. Mills, and A. C. Naveira Garabato (2013), Rapid cross-density ocean mixing at mid-depths in the Drake Passage measured by tracer release, *Nature*, *501*(7467), 408–411.

Wu, L., Z. Jing, S. Riser, and M. Visbeck (2011), Seasonal and spatial variations of Southern Ocean diapycnal mixing from Argo profiling floats, *Nat. Geosci.*, *4*(6), 363–366.

Wunsch, C., and R. Ferrari (2004), Vertical mixing, energy, and the general circulation of the oceans, *Ann. Rev. Fluid Mech.*, *36*(1), 281–314, doi:10.1146/annurev.fluid.36.050802.122121.

Zhai, X., H. L. Johnson, D. P. Marshall, and C. Wunsch (2012), On the wind power input to the ocean general circulation, *J. Phys. Oceanogr.*, *42*(8), 1357–1365, doi:10.1175/JPO-D-12-09.1.